https://doi.org/10.1016/j.resconrec.2022.106665

Utilization of contaminated air pollution control residues generated from sewage sludge incinerator for the preparation of alkali-activated materials

Keke Sun, Hafiz Asad Ali, Weiyi Ji, Jiaxing Ban, Chi Sun Poon*

Department of Civil and Environmental Engineering, The Hong Kong Polytechnic University, Hung Hom, Kowloon, Hong Kong, China

Corresponding author: cecspoon@polyu.edu.hk

Abstract: The air pollution control (APC) residues from the sewage sludge incinerators are harmful to the environment due to their relatively rich soluble salts and heavy metal content. In this paper, the APC residues were pre-treated by water washing at the different liquid to solid ratios (L/S), and a ternary contour diagram was introduced to optimize the composition of slag, waste glass powders and APC residues in alkali-activated materials (AAMs). The result showed that the washing method could remove sulfate of APC residues, while the heavy metals and chloride required a higher L/S ratio to achieve a higher removal rate. Incorporation of the APC residues reduced the compressive strength of AAMs mortar, but the AAMs prepared with the washed APC residues showed a higher compressive strength than the unwashed APC residues. The sulfate from the unwashed APC residues can be used as an activator to improve the drying shrinkage of the AAMs due to the formation of ettringite, while the washed APC residues can be used as a precursor of the AAMs due to the rich aluminosilicate content. The leaching test results indicated that up to 30% washed APC residues incorporated into AAMs showed little leaching of heavy metals. On the contrary, when more than 10% unwashed APC residues are used, the pre-treatment is necessary before they can be utilized for preparing AAMs due to the leaching of heavy metals.

Keywords: Recycling; washing; APC residues; waste glass powder; heavy metals; alkali-activated materials.

1. Introduction

Alkali-activated materials (AAMs), as a product of aluminum-silicon precursors reacting with strong alkali solutions, are considered as potential alternatives to ordinary Portland cement

due to their comparable mechanical properties and durability, low CO_2 emissions and energy consumption during manufacturing (Davidovits, 2013; Duxson et al., 2007; Provis et al., 2009). Many solid wastes with rich aluminium-silicon contents (e.g., fly ash, ferrous slag, non-ferrous metallic slag, etc.,) could be large-scale utilized as raw materials to produce sustainable AAMs via their good alkali-activation potentials (Shi et al., 2000; Sun et al., 2021; Van Sande et al., 2020). However, in some regions, the availability of high-quality precursor materials is limited due to growing environmental concerns and diminishing heavy industries. For instance, in Hong Kong, coal-fired power plants will be phased out soon due to pressure on reducing CO_2. Therefore, using locally available alternative raw materials as the precursors of the AAMs is promoted to reduce the accumulation of industrial waste and CO_2 emissions.

In Hong Kong, waste glass contributes to a significant proportion of municipal solid waste (291 tonnes/day in 2017), but only 20% of waste glass could be recycled due to the lack of a glass manufacturing industry (Ling et al., 2013). As a potential alkali-siliceous material, waste glass powder (GP) had been investigated extensively as potential raw material to produce the AAMs (Pascual et al., 2021). Due to GP's lower activation and reactive alumina content, a significant strength reduction of the alkali-activated GP was reported compared to alkali-activated slag or fly ash (Redden et al., 2014). In previous studies, it was demonstrated that the combined use of glass powder and slag could provide sufficient Ca and Al to form stable C-(N)-A-S-H gels and compensate for the strength loss of such AAMs (He et al., 2020a; He et al., 2021b; Zhang et al., 2020). Therefore, the beneficial reuse of waste glass powders in AAMs manufacturing provides significant economic and environmental benefits, and there is still increasing demand for such sustainable materials.

Moreover, approximately 1,200 tonnes of sewage sludge are produced daily in Hong Kong (Swann et al., 2017). The Hong Kong government has constructed the world's largest sewage sludge incinerator to incinerate a maximum of 2,000 tons of dewatered sewage sludge a day, reducing the waste volume by almost 90% and waste mass by 70%. But this disposal solution to the sewage sludge still generates a new problem, namely disposing the incineration sewage sludge ash and air pollution control (APC) residues. Landfill disposal of these solid wastes is inadvisable due to occupying the valuable land resources and wasting the recoverable resources. Research on reusing incineration sewage sludge ash has provided some feasible solutions for the recycling of the incineration fly ash. An approach is to make the AAMs by co-disposing incineration sewage sludge ash, with pozzolanic waste, such as metakaolin, granulated ground blast furnace slag or fly ash (Chen et al., 2018; Hadas, 2021; Longhi et al., 2022). Additionally, depending on the characteristics of the sewage sludge, which is incinerated, the APC residues usually contain a high content of chlorides, sulfates, and heavy metals (Quina et al., 2010a; Rani et al., 2008a). Recent studies have investigated the possible use of the sulfate from the

solid waste fly ash as mineral feed for cement manufacture or as activators for slag (Lampris et al., 2009; Ren et al., 2021; Sun et al., 2022a), but the high contents of sulfate and chloride in the incineration sewage sludge fly ash would have negative impacts on the durability of cementitious materials, such as causing steel corrosion and expansion due to the formation of ettringite (Cai et al., 2021a; Cai et al., 2022b; Gunasekara et al., 2019; Sun et al., 2022b). In addition, as a potentially hazardous waste, improper disposal of the APC residues would cause adverse effects on human health and environmental concerns. Several studies have reported AAMs as construction materials can be used to solidify/stabilize the heavy metals of the contaminated sewage sludge fly ash (Wang et al., 2010; Ren et al., 2021). Therefore, recycling of the APC residues in the AAMs not only reduced the burden of landfills, but also eliminated the potential environmental risks due to the leaching of heavy metals. To reduce the detrimental effects of soluble salts and heavy metals of the APC residues, a pre-treatment washing step of these residues with water was commonly adopted (Bayuseno et al., 2011; Bogush et al., 2019a; Quina et al., 2008b). However, little information on the fundamental characteristics of the washed and unwashed APC residues, such as the physical and chemical characteristics and the leaching behavior of heavy metals, is available.

To stabilize the heavy metals and soluble salts of the APC residues and maximize the recycling rate of the APC residues, a solidification/stabilization process using one-part AAMs is proposed. The current study aimed to determine the effect of the liquid/solid ratio during the washing process on the chemical composition of the APC residues before final stabilization/solidification. The washed and unwashed APC residues, recycled waste GP, and slag were used as the precursors of the AAMs, and a ternary contour diagram of the mixing design was used to determine its optimal mixing design ratio. In addition, the effect of the washed and unwashed APC residues on the mechanical and microstructure properties of the AAMs and the leaching behavior of heavy metals were assessed. This research finding would facilitate the recycling of the APC residues and waste GP as precursors in AAMs, which would directly reduce the demand for cement and concrete in virgin construction materials.

2. Raw materials and experimental methods

2.1 Raw materials

A combination of ground granulated blast-furnace slag, waste glass powder (GP), and air pollution control (APC) residues are employed as precursors to prepare the one-part alkali-activated materials (AAMs), and a commercial solid sodium silicate composed of 35.8% Na_2O and 62.9% SiO_2 was used as the alkali activator. As-received APC residues were collected from a local sewage sludge incinerator (Sludge Treatment Facilities, T-park, Hong Kong), and the waste glass cullet was collected from a local beverage bottle recycler. Prior to use, the as-received APC residue and waste glass cullet were dried at 105 °C for 48 hours and then milled

separately for 2 hours and 1.5 hours. The chemical compositions and particle size distributions of the slag and GP are shown in Table S1 and Fig. S1, respectively. The as-received APC residues were washed with liquid/solid ratios (L/S) of 1:1, 5:1, and 10:1 by immersing them in water at the respective L/S ratios for 12 hours to remove soluble salts. The washed APC residue was separated by a centrifuge at 3000 rpm, and the basic chemical and physical information of the APC residues before and after washing are presented in Section 3.1. Based on the removal ratio of soluble slats, the APC residues washed with L/S of 10:1 were selected to prepare the AAMs.

2.2 Experimental methods

2.2.1 Mixing proportion

One-part alkali-activated pastes and mortars are generally prepared by just adding water into the pre-mixed dry precursors and solid activators. Here, a design method for the ternary composites was used to design the relative proportions of the slag, waste GP and APC residues in the one-part AAMs. It had been confirmed that this method was a valuable tool for achieving the optimal mixing proportions of multiple system cementitious materials with desired physical and durability properties (He et al., 2020a; Hu et al., 2017; Sun et al., 2019). Fig. S2 shows the mixing proportions of all 21 prepared AAM samples in this study, and based on the chemical composition and mixing proportions, the Na_2O/Al_2O_3, SiO_2/Al_2O_3 and CaO/SiO_2 molar ratios of each design mix are presented in Table S2. All AAM mortars were prepared with a water/binder ratio of 0.3 and the activator/binder mass ratio of 0.1 (Sun et al., 2022a). River sand with the fineness modulus of 2.1 was used as the aggregate, and the sand/binder ratio was 1.0. These precursors, activator and river sand were first mixed for 2 min in a mechanical mixer, and then water was directly added to the dry powders to mix for the other 3 min. The same water/precursors ratio but without sand was used to prepare the AAM pastes for the microstructure tests. The freshly AAM paste and mortars were cast into moulds and were transferred into a curing room (25℃ and relative humidity of 95%). After one day, these specimens were demoulded and continuously cured in the same curing room until further testing. The contour lines of the fluidity, compressive strength and drying shrinkage of AAMs could be obtained by the software of the Expert Design.

2.2.2 Fluidity and compressive strength

The fluidity of the freshly AAM mortars was assessed in accordance with the ASTM C1437 (ASTM C1437). A truncated conical mould was filled with the fresh mortar, and the fluidity was recorded as the spread of the cone after 25 vibrations. The fresh mortars were cast into 40 mm× 40 mm× 40 mm plastic moulds for the compressive strength test, conducted by a hydraulic compressive machine with a loading rate of 0.5 MPa/s following the ASTM C109 (ASTM C109).

142 2.2.3 Drying shrinkage

143 The freshly AAM mortars were cast into 25 mm×25 mm×285 mm steel moulds for the
144 drying shrinkage test. After 24 hours, the initial length of mortar bars was immediately recorded
145 by a comparator, and then the bars were moved into a chamber with 25±2 °C and relative
146 humidity of 50%. The 28 days drying shrinkage of the AAM mortars was calculated by the
147 length changes.

148 2.2.4 Heavy metals of APC residues and AAMs

149 The total heavy metal contents of the APC residues were tested by the aqua regia digestion
150 method (USEPA 3050B). Air-dried APC residues were ground and allowed to pass through a
151 45μm sieve, and about 1g of the APC residues was digested into the 10 mL aqua regia for two
152 days. In addition, a toxicity characteristic leaching procedure (TCLP) was used to evaluate the
153 leaching risk of the AAMs prepared with the APC residues according to the EN12457 and
154 USEPA 1311. The 28 days ground AAMs powders about 1±0.1g were respectively mixed with
155 deionized water and glacial acetic acid (pH=2.88) at a liquid/solid ratio of 20:1 and tumbled for
156 18 hours. The leaching solution of the APC residues and AAMs were filtrated through 0.45μm
157 membrane filters. The heavy metal concentration was tested using an inductively coupled
158 plasma/optical emission spectroscopy (ICP-OES, FMX36, SPECTROBLUE). Before
159 measurement, the digestions of the leaching solution were carried out by a digestion block at
160 105℃ to evaporate to dryness. After evaporation to near dryness, the sample was diluted with
161 5% nitric acid.

162 2.2.5 Microanalysis

163 The central part of the AAM pastes was soaked in ethyl alcohol to stop the alkali-activated
164 reaction. Before microanalysis tests, the samples were dried at 40℃ for a week in a vacuum
165 oven. The gold-coated specimens were employed for the SEM/EDS analyses (Tescan VEGA3).
166 Besides, X-ray diffractometry (XRD, Rigaku Smart Lab-Advance) was used to characterize the
167 crystalline phases of the reaction products of AAMs. The scan range, step size, and dwelling
168 time of this test were 5°~70°, 0.02° and 1s, respectively.

169 3. Results and discussions

170 3.1 Effect of L/S ratios on the APC residues

171 Table 1 shows the chemical compositions of the as-received APC residues and washed
172 APC residues. From Table 1, the as-received APC residues were mainly composed of the 35.1%
173 Na_2O, 33.0% SO_2, and 4.11% Cl. The high sodium sulfate content in the as-received APC
174 residues resulted from the removal of gaseous SO_2 accomplished by using sodium bicarbonate
175 in the flue gas treatment process. Besides, the amount of 4.11 wt.% Cl and 5.12% of Fe_2O_3 in
176 the as-received APC residue were attributed to using seawater in toilet flushing and the use of
177 $FeCl_3$ in the chemically enhanced primary treatment process at the sewage treatment plants in

178 Hong Kong. After washing, the Na_2O, SO_2 and Cl content of the APC residues decreased
179 significantly with an increase in the L/S ratios. The result illustrated that the Cl and S elements
180 as water-soluble constituents in the APC residues were easily washed away when contacting
181 water. The removal efficiency of the sulfate and chloride salts of the washed APC residue with
182 the L/S of 1 was 44.2% and 7.3%, respectively, and increasing the L/S ratio enhanced the
183 removal efficiency of the soluble salts. The removal efficiency of the sulfate and chloride salts
184 in the APC residues washed with L/S of 5 was 70.0% and 28.2%, respectively, which were
185 further increased to 84.5 % and 81.5%, respectively, when the L/S of 10 was used. The result
186 illustrates that the low L/S ratio can remove most of the sulfate from the as-received APC
187 residues, while the chloride salts required a higher L/S ratio for their removal. Furthermore, the
188 removal efficiency of sulfate salt was higher than that of chloride, which was contrary to the
189 previous studies on the APC residues (Bogush et al., 2019a; Chimenos et al., 2005; Yang et al.,
190 2017). This is probably due to the differences in chemical compositions and solubility constants
191 of these salts in the as-received APC residues. In the previous literature (Bogush et al., 2019a;
192 Chimenos et al., 2005; Yang et al., 2017), most chlorides in the APC residues were present in
193 the form of soluble alkali chlorides, but the insoluble sulfates were present mainly in form of
194 insoluble salts (i.e. $CaSO_4$), which was ascribed to the addition of lime for flue-gas treatment.
195 After washing, most chloride could be removed, while a large percentage of sulfate was still
196 preserved in the APC residues. However, the sulfate and chloride present in these APC residues
197 was mainly the soluble Na_2SO_4 and NaCl as shown in Fig. 1(a), and the Na_2SO_4 (40.8g/100g)
198 showed a higher solubility than NaCl (35.7g/100g) at 25℃, meaning a high removal efficiency
199 of sulfate by washing (Krumgalz, 2017).

200 The Al_2O_3, SiO_2 and CaO in the APC residues increased with the increase in the L/S ratio.
201 The rich alumina-silicate in the washed APC residues could become a potential precursor to
202 produce the AAMs, and a similar result was reported when direct current (DC) plasma arc
203 technology was used to treat the APC residues. The DC plasma treatment of the APC residues
204 significantly reduced the heavy metals and soluble salts, and the residual amorphous glassy
205 phases can achieve a high strength of geopolymer composites (Kourti et al., 2010; Rani et al.,
206 2008b). In addition, the total organic carbon (TOC) of the APC residues slightly decreased with
207 the increase of the L/S ratio, and the lower removal efficiency of the TOC was mainly due to
208 the insolubility of the organic matters in water. Nevertheless, the inorganic carbon (IC) content
209 in the washed APC residues was increased when the L/S ratio of 10 was used. This could be
210 attributed to an increase in the relative content of insoluble carbonate caused by the loss of the
211 soluble salts in the APC residues during the washing process.

212 Fig. 1(a) shows the XRD pattern of as-received APC residues and washed APC residues.
213 The XRD patterns of the washed and unwashed APC residues were significantly different. The

XRD pattern of the as-received APC residues showed the peaks of Na_2SO_4 and NaCl. Both NaCl and Na_2SO_4 dissolved during the washed process, and so their peak intensities were significantly decreased in the washed APC residues. Besides, a small hump at around 25°~35° was found in the washed APC residues, and it was associated with amorphous aluminosilicate. The phase of albite and Fe_2O_3 were also identified. Furthermore, there were some peaks of $Ca(OH)_2$ in the washed APC residues, which was attributed to the decomposition of the $CaCl_xOH_{2-x}$ phases during the washing process. The $Ca(OH)_2$ remained in the washed APC residues because of its low solubility (Wang et al., 2010; Bogush et al., 2015b). Fig. 1(b) shows the effect of the L/S ratios on the thermal stability of the as-received APC residues and washed APC residues. The mass loss of the APC residues was stable before 500°C, and the total mass loss of the as-received APC residues from 50°C to 1000°C was 20.6%. However, there was an increase of the total mass loss for the washed APC residues with the increase of the L/S ratios, and this could be ascribed to the presence of residual water after washed. The minor peaks between 550°C~630 °C corresponded to the decomposition of the $CaCl_xOH_{2-x}$ phase, with a mass loss of 0.4%. Moreover, the major mass loss between 700~800°C and 850~1000°C was primarily due to the decomposition of carbonate and the evaporation of soluble chlorides salts (Rani et al., 2008b). It was however noted that the carbonate was not detected by the XRD probably due to its amorphous structure formed during the experiment. The mass loss of the washed APC residues at 850~1000°C decreased with the increase of the L/S ratios due to the reduction of soluble chlorides after washing.

Table 2 shows the effect of the L/S ratio on the leaching of the total heavy metals from the APC residues. It could be seen that the as-received APC residue contained various heavy metals with relatively higher concentrations of Zn and Sr, followed by Pb, Cu, As, Ag, and Se. The different L/S ratios had an insignificant influence on the leaching behavior of the various heavy metals, illustrating that the heavy metals of the APC residue were incorporated into the sintered matrix. However, the concentration of Cr, Cu and Zn reduced when the APC residues were washed with the L/S ratios of 10. This phenomenon was because the extracting behavior of these heavy metals was dominated by reaction kinetics and the pH value of the solution during the washing process. The formation of $Ca(OH)_2$ from the hydrolyzation of the $CaCl_xOH_{2-x}$ phase provided an alkaline condition, and in this relatively higher pH environment, the amphoteric metals such as Zn form complex ion solutes with high solubility (Wang et al., 2010; Bogush et al., 2015b).

Table 1 Compositions of the APC residues before after washing with the different L/S (wt.%)

	Na_2O	MgO	Al_2O_3	SiO_2	P_2O_5	SO_3	Cl	K_2O	CaO	Fe_2O_3	Others	TOC	IC
As received	35.1	1.83	4.64	7.56	3.52	33	4.11	0.67	3.78	5.12	2.48	2.41	1.37
1:1	24.4	3.10	8.81	13.9	7.00	18.4	3.81	1.18	7.34	9.90	2.16	2.01	1.50
1:5	14.7	3.68	11.2	17.8	9.84	10.8	2.96	1.55	10.7	15.2	1.57	2.08	2.12

1:10	9.05	4.34	13	20.7	11.8	5.13	1.24	1.71	12.6	18.6	0.12	1.73	4.92

TOC: Total Organic Carbon; IC: Inorganic Carbon.

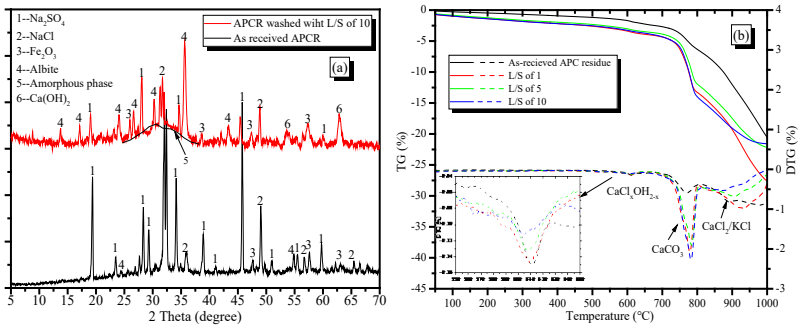

Fig. 1 Information of as-received APC residues and washed APC residues (a) XRD and (b) TG/DTG

Table 2 Total heavy metal of the APC residues extracted by the aqua regia (mg/kg)

	Ag	As	Ba	Cd	Co	Cr	Cu	Mn	Mo	Ni	Pb	Sb	Se	Sn	Sr	Zn
As received	11.9	17.2	3.3	0.75	2	6.4	13.8	3.9	3.3	4.1	17.5	8.5	13.6	4.9	17.1	32.5
L/S=1:1	11.5	19.4	3.7	0.58	2.3	9.4	21.8	9	3.3	5.6	19.3	9.1	14.3	5.7	22.1	73
L/S=1:5	11.6	20.6	8.1	0.62	2.3	11	26.4	10.7	3.4	6.2	20.6	9.4	14.5	7.1	25.5	97
L/S=1:10	11.3	15.3	1.2	0.44	1.9	3.9	7.6	0.5	3	3.3	16.7	8.3	13.7	3.9	13.3	3.4

3.2 Fluidity

The effect of washed and unwashed APC residues on the fluidity of the AAM mortars is shown in Fig. 2. From Fig. 2(a), the fluidity of AAMs mortar increased with the increase of the GP content and decreased with the increase of washed APC residues. As shown in Fig. 2(b), a similar trend was found when the unwashed APC residues were used. The improvement of the fluidity was related to the smooth surface and non-absorbent nature of GP which meant that more free water was available for inter-particle lubrication (Liang et al., 2021; Shoaei et al., 2020). However, the reduction of the fluidity can be explained by the irregular and rough texture of the APC residues particles. The irregular shape increased the friction, and the rough texture also favored the adsorption of water (Pan et al., 2003). At the same fluidity, a higher content of the washed APC residues can be incorporated than the unwashed APC residues. This was because the high concentration of soluble salts in the unwashed APC residues, e.g., Na_2SO_4 and NaCl, increased the surface tension of pore solution, which resulted in greater agglomeration particles and slippage resistance.

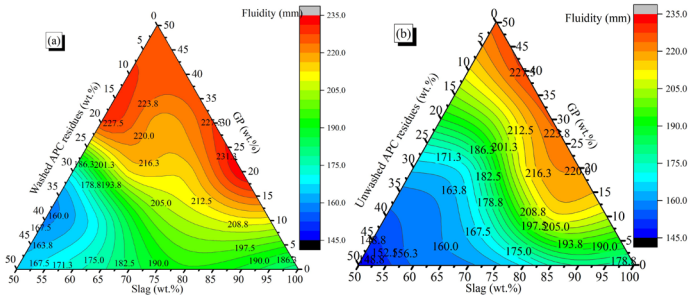

Fig. 2 Effect of (a) washed and (b) unwashed APC residues on the fluidity of AAM mortars

3.3 Compressive strength

The effects of the unwashed and washed ACP residues on the compressive strength of the AAM mortars are shown in Fig. 3. The compressive strength of the AAMs mortar increased with the increased curing ages, and the compressive strength decreased with the increase of the washed and unwashed APC residues. From Fig. 3(a) and (b), two regions can be noticed to correspond to the higher and lower compressive strength of the AAM mortars. For 28 days compressive strength (Fig. 3(a)), the mixing proportion in the region with a high strength occurred in the AAM mortars prepared with 80%-90% slag content, 0-20% GP content, and less than 0-10% unwashed APC residues content. The optimum proportion of the ternary component was 70% slag, 25% GP content, and 5% unwashed APC residues and the resulting compressive strength could reach 72MPa at 28 days. While, regarding the AAM mortars prepared with washed APC residues in Fig. 3(b), the highest strength region occurred with 70-90% slag, 0-30% GP and less than 20% washed APC residues content. The highest compressive strength of the AAMs was prepared with 65% slag, 20% GP content, and 15% washed APC residues and it could reach 90MPa at 28 days.

For the AMMs prepared with APC residues, regardless of using the washed and unwashed APC residues, the lower strength region of the AAM mortars occurred when less than 70% slag was used, but the compressive strength of all mortars was higher than 40 MPa at 28 days. Considering similar proportioning of the ternary precursors, the AAMs prepared with washed APC residues could achieve higher compressive strength than the unwashed APC residues, implying that the washed APC residues had better activation potential than the unwashed APC residues. The reason could be that the relative amount of amorphous aluminosilicate phases was increased in the washed APC residues, which contributed to the formation of more reaction products. In addition, the organic carbon in the unwashed APC residues had a negative effect on the compressive strength of AAMs due to its inhibiting effect on the reaction (Diab et al., 2016; Chen et al., 2020).

The early compressive strength of the AAM mortars increased with the increase of the GP content (up to about 25%) and then decreased when the GP content exceeded this ratio. The enhancement of the GP on the compressive strengths was because of its filling effect, but this reduction could be attributed to the lower activation than that of slag (Liu et al., 2019; Ali et al., 2020). The large amount of slag and GP contributed to the high-early compressive strength of the AAMs, but it had been noted that the 28 days compressive strength of the AAMs prepared with more than 95% slag would be reduced, which was also reported in many previous studies (Collins et al., 2001; Hubler et al., 2011; Zhang et al., 2020). The reason was due to the high

shrinkage deformation and microcracking of the AAMs (Bakharev et al., 1999; Hubler et al., 2011). Therefore, incorporating the washed and unwashed APC residues decreased the compressive strength of AAM mortar, but the later compressive strength showed a continuously increasing trend.

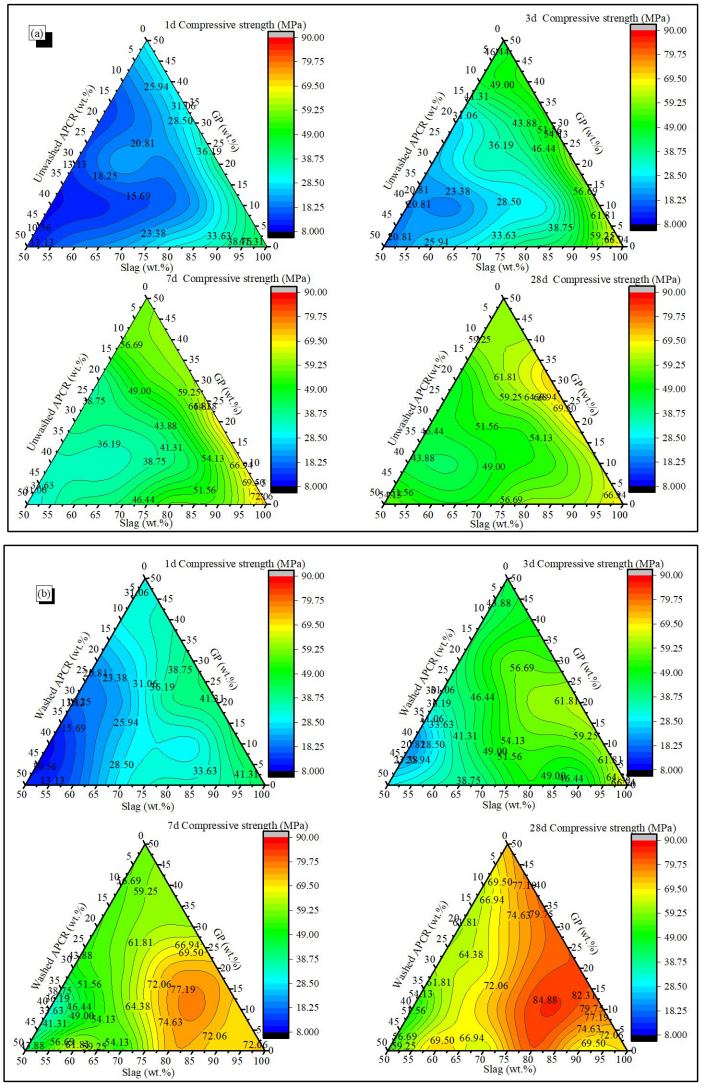

Fig. 3 Effect of (a) unwashed and (b) washed APC residues on the compressive strength of AAM mortars

3.4 Drying shrinkage

Fig. 4 shows the contour lines of the drying shrinkage of the AAM mortars prepared with washed and unwashed APC residues at 28 days. It can be seen in Fig. 4(a) and (b) that the slag content in the ternary system largely governed the drying shrinkage of AAMs. The drying shrinkage of the AAMs increased with the increase of slag content, and the shrinkage magnitude among these samples was more than 10,000 micro strains. The addition of the GP and APC residues affected the shrinkage behavior of the AAMs differently. Fixing the slag content in the contour plots, the addition of washed or unwashed APC residues reduced the drying shrinkage

of the AAMs when the replacement level was higher than 10%, while the drying shrinkage was slightly increased when less than 35% GP replacement was used in the mix proportion. But the drying shrinkage slightly decreased when the GP content continuously increased. It could be seen from the results that the APC residues were more effective to reduce the drying shrinkage of AAMs than GP due to the lower reactivity.

Considering similar proportion of the ternary precursors, the drying shrinkage of the AAMs prepared with the washed APC residues were 10%~30% higher than that of the samples prepared with the unwashed APC residues. The lowest drying shrinkage was about 1,400 micro strains and 1,500 micro strains when 45% unwashed APC residues and 35% washed APC residues were added, respectively. It could be concluded that the unwashed APC residues had a better shrinkage-reducing effect than the washed APC residues. The reason was probably due to the rich sulfate ion presence in unwashed APC residues reacting with the dissolved aluminum phases from the precursors to form expansive ettringite, which could compensate for the drying shrinkage. The formation of the ettringite combined with many moistures, meaning a reduction of the evaporate moisture and capillarity pressure (Nagataki et al., 1998). Meanwhile, the ettringite crystal developed within the capillary pores and hence produced expansive stress to reduce the drying shrinkage of AAMs and a similar finding was reported in the literature (Nguyen et al., 2019). Besides, it had also been reported that a substantial volume increased by about 315% occurred during the transformation of anhydrous sodium sulfate to its hydrous form (Thaulow et al., 2004).

As shown in Fig.3 (a) and (b), the 28 days compressive strength of the AAMs prepared with a high slag content showed slightly decreased, and correspondingly it also showed the highest drying shrinkage as shown in Fig.4 (a) and (b). Besides, the mixing proportions with a stable strength development had lower drying shrinkage. Therefore, the study results showed the drying shrinkage of the AAMs prepared with a high slag content could suffer risks of shrinkage-cracking. The addition of the unwashed and washed APC residues presented an indirect positive effect on the compressive strength due to the less shrinkage-cracking.

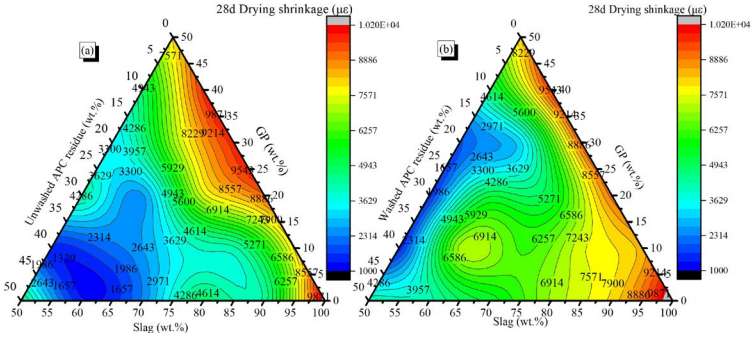

Fig. 4 Effect of (a) unwashed and (b) washed APC residues on drying shrinkage of AAM mortars

3.5 Leaching behavior of AAM pastes

As shown in Table 2, the high concentrations of heavy metals (especially for Zn, Pb, Cu and As) were present in the washed and unwashed APC residues and were of greater importance concerning the environmental impact of the materials. Table 3 summarizes the leaching results of heavy metals from the AAMs prepared with the heavy metal-containing washed and unwashed APC residues, and the leachability is compared with the TCLP limits and BS EN12457 limits. From Table 3, when the AAMs prepared with the washed and unwashed APC residues were exposed to deionized water, the heavy metals showed a higher concentration of Se, followed by Zn, Ag and Sb. Though the concentration of most heavy metals in water would pass the EN 12457 waste acceptance criteria, the concentration of Se and Sb would fail to meet the regulatory limits. However, regardless of the washed and unwashed APC residues, the concentration of heavy metals leached from the AAMs was greatly reduced compared to the total content of heavy metals (as shown in Table 2). The results illustrated that the AAMs prepared with a large amount of the washed and unwashed APC residues were less effective at immobilizing Se and Pb, but the other heavy metals, including the Ba, Cd, Co, Cr, Mo and Ni were almost fully immobilized. The lower concentration of heavy metals from AAMs was ascribed to the pore solution with a high pH environment (~13), which stopped the dissolution of heavy metals. A similar leaching test result was observed when the AAMs were immersed in the acetic acid. However, it was noted that the AAMs in the acetic acid showed higher concentrations of heavy metals compared to that in deionized water. This could be attributed to the pore solution of AAMs in the acetic acid having a lower pH value due to neutralization, which accelerated the release of heavy metals. The results illustrated that the risk of heavy metal leaching may not be negligible when AAMs prepared with the APC residues were used in some acid-corroded environments, such as sewerage structures. In addition, in the water and acid, the leaching of heavy metals from the AAMs prepared with the unwashed APC residues was higher than that of washed APC residues. The heavy metals concentrations of the AAMs prepared with less than 30% washed APC residues did not exceed the TCLP regulatory limitation. However, when 50% unwashed APC residue was used, the leaching of certain heavy metals (e.g., Ag, As and Ni) was higher than the TCLP regulatory limits. This indicates that the use of the unwashed APC residues might increase the risk of heavy metal leaching, but the risk was negligible for the AAMs when less than 30% washed APC residues were used. Therefore, the AAMs can efficiently immobilize the heavy metals of the washed APC residues even at a higher percentage. In addition, the TCLP method was usually designed to estimate the worst-case leaching conditions of disintegrated landfilled wastes. However, the AAMs were usually used as construction materials with monolithic shapes. In our previous results (Sun et al., 2022a), the

TCLP method was used to test AAMs crushed to a size of 2mm-3mm to simulate scenarios of construction materials with monolithic shapes, and the concentrations of the leached heavy metals were far below the TCLP regulatory limits. In this study, the TCLP test results of AAMs particles with the size of 2mm-3mm showed lower concentrations than those samples with a size of 45μm, further proving that the problem of environmental pollution could be significantly minimized when the AAMs with the unwashed APC residues were used as construction materials.

Table 3 Leaching concentrations of AAMs with washed and unwashed APC residue (mg/L)

		Ag	As	Ba	Cd	Co	Cr	Mn	Mo	Ni	Pb	Sb	Se	Zn
Deionized water	50S50U	5.45	4.83	1.86	2.05	0.46	1.59	7.80	-	3.30	5.05	4.66	7.35	6.10
	50S50W	4.75	4.98	2.05	2.62	0.27	1.20	0.72	0.57	3.50	4.59	4.52	7.45	3.31
	50S20G30U	5.35	5.10	-	1.61	-	1.60	-	-	3.51	3.82	4.53	3.25	2.41
	50S20G30W	3.05	4.81	-	0.28	-	1.03	-	2.09	3.42	3.8	4.64	1.21	-
	60S30G10U	1.25	1.56	-	0.10	-	1.63	-	-	-	4.87	4.39	1.40	0.32
	60S30G10W	1.55	1.20	-	0.84	-	0.24	-	-	-	2.99	3.28	0.05	-
	50S30G20U	4.02	3.49	-	0.69	-	0.29	-	-	3.70	3.16	3.48	5.10	-
	50S30G20W	3.72	1.35	-	0.74	-	-	-	-	3.61	2.83	3.19	0.85	-
EN 12457 limits		-	2	100	1	-	10	-	10	10	10	0.7	0.5	50
Acetic acid (pH=2.88)	50S50U	6.01	11.3	0.22	1.59	0.98	3.54	8.63	-	1.06	7.99	5.91	11.81	6.52
	50S50W	3.84	7.10	0.23	1.33	0.33	1.91	4.90	-	-	4.08	4.66	8.34	5.94
	50S20G30U	5.85	10.7	0.42	1.76	0.97	3.61	1.59	-	1.15	4.24	5.26	3.16	6.57
	50S20G30W	4.62	1.40	0.21	0.40	0.52	2.28	2.50	-	-	9.54	2.62	1.59	6.10
	60S30G10U	4.08	2.20	0.15	0.36	0.37	1.86	9.46	-	-	8.23	0.92	1.77	5.87
	60S30G10W	3.56	0.60	1.12	0.32	0.33	1.79	2.61	-	-	8.10	0.84	0.52	4.69
	50S30G20U	4.10	4.40	0.16	1.09	0.96	3.48	0.92	0.34	1.02	3.82	1.38	2.76	6.09
	50S30G20W	3.79	0.55	0.21	0.88	0.37	1.92	1.65	-	-	8.27	0.36	1.06	5.89
TCLP limits		5	5	100	1	1	5	-	-	-	5	-	1	-

"-": no detected. The S, G, W and U refers to slag, glass powder, washed and unwashed APC residues, and the number refers to the content of the precursor.

3.6 Reaction heat

The effect of the APC residues on the heat flow and cumulative heat of the alkali-activated slag/GP is illustrated in Fig. 5. From Fig. 5(a), in one-part AAMs, two exothermic peaks can be observed for the alkali-activated slag/GP. The initial exothermic peak (peak I) occurred after mixing with water due to the wetting and dissolution of the precursor and solid alkali, and the second exothermic peak (peak II) was attributed to the formation and precipitation of initial C-(N)-A-S-H gels. An induction period varying from 5 h to 10 h was found between peak I and peak II. When the unwashed or washed APC residues were used, the duration of the induction period was reduced by 45%~65%. The alkali metal from the APC residues accelerated the breaking of the Ca-O, Si-O and Al-O bond of slag and GP due to its strong polarization effect, and the rich aluminium and silicate units contributed to the precipitation of gels (Patel et al., 2018; Sun et al., 2022). It was noted that the third exothermic peak (peak III) and longer dormant periods between peaks II and III were found in AAMs with unwashed APC residues. During this stage, the sulfate of the APC residues could react with the dissolved aluminum and

calcium to form ettringite or layered double hydroxides, corresponding to peak III. The peak III was also found in the AMMs with 50% washed APC residues since the existence of high sulfate content. Therefore, the sulfate from the APC residues can be used as a weak alkaline activator to improve the drying shrinkage of AAMs.

From Fig. 5(b), the total cumulative heat of the alkali-activated slag/GP decreased with the increase of the APC residues. This reason can be attributed to the retarding effect of a high concentration of sodium chloride in the system (Brough et al,. 2000). In addition, the AAM prepared with the washed APC residues showed a higher cumulative heat than that of the unwashed APC residues, illustrating a higher reaction activity of the washed APC residues. This is because a large amount of the silicate and aluminate from the washed APC residues were able to contribute more to the geopolymerization than that of the unwashed APC residues.

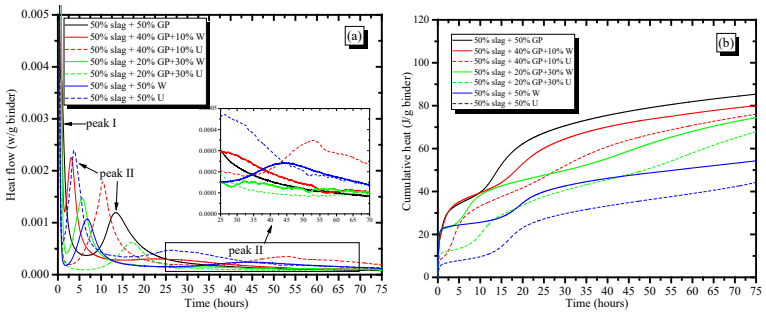

Fig. 5 Effect of APC residue on the heat flow and cumulative heat of alkali-activated slag/GP

3.7 XRD

The XRD patterns of the precursors and alkali-activated slag/GP at 28-days are shown in Fig. S3. The GP and slag showed an amorphous hump at 20°~30° and 25°~35°, respectively, and the stable anorthite in the slag was also found. A broad hump was present in the patterns of the AAMs at 25°~35° 2θ, corresponding to a low crystallinity amorphous gel. It had been reported that the main reaction product of the alkali-activated slag was the C-A-S-H gels, and incorporation of the soda-lime-silica glass powders into the alkali-activated slag favored the formation of N-A-S-H gels (He et al., 2021b; Pascual, et al., 2021). The coexistence of the C-(A)-S-H and N-A-S-H gels in the AAMs had been reported previously, but these gel phases were difficult to be identified via the XRD due to their amorphous nature and the presence of other crystalline phases (Garcia-Lodeiro et al., 2011; Walkley et al., 2016). A low-intensity peaks at 11.3° and 21.5° 2θ were identified as hydrotalcite phase with a layered double hydroxide structure.

Fig. 6 shows the XRD patterns of the AAM prepared with the washed and unwashed APC residues. The AAMs prepared with 10% washed and unwashed APC residues showed a broad hump at 25°~35°, illustrating the formation of amorphous gels. The peaks of the sodium sulfate and sodium chloride were observed in AAMs prepared with more than 10% APC residues, and

the incorporation of the washed APC residues in the AAMs lowered the peak intensity of sulfate and chloride. The peak of sodium sulfate could barely be found in AAMs prepared with 10% unwashed or washed APC residues, and new crystalline phases of ettringite and Friedel's salts as secondary reaction products were found when more than 30% unwashed or washed APC residues were used. The results illustrated that sodium sulfate from the APC residue could be consumed during the alkali activation reaction. The ettringite formation could result in crystallization stress leading to a reduction in shrinkage of the AAMs, as shown in Fig. 4. Notably, when 10% and 20% unwashed APC residues were incorporated in AAMs, there was no sulfoaluminate phase detected (or extreme low intensity of the peaks). This could be due to the decrease in the amount of reactive Al_2O_3 and CaO of the precursors. With the increase of GP and APC residues contents, the limited content of Al_2O_3 and CaO from the slag could be rapidly exhausted by the formation of the poorly crystalline AFm or hydrotalcite phases. The XRD did not identify these minor crystalline phases in the alkali-activated slag/GP, and similar results were reported in previous studies (He et al., 2021b; Mobasher et al., 2016). In addition, the washed APC residues with a lower reactivity would induce a large amount of residue alkali in the pore solution, and so the absence of AFt was most likely due to the high alkalinity of the alkali pore solution (about pH~13) preventing the formation of ettringite (Mobasher et al., 2016; Uppalapati et al., 2020).

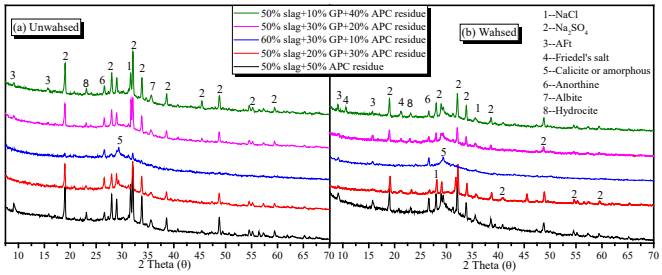

Fig. 6 XRD patterns of AAMs with washed and unwashed APC residues at 28 days

3.8 SEM/EDS

The SEM/EDS micrographs of the AAMs prepared with the washed and unwashed APC residues at 28 days are shown in Fig. S4. The image of AAMs showed a large number of gels, while the alkali-activated slag (100S) and slag/GP (50S50G) showed the presence of microcracks, which was closely related to the higher drying shrinkage as discussed above. Besides, a large amount of unreacted GP with a lower activity was wrapped by a continuous amorphous phase in the 60S30G10W and 60S30G10U, which were identified by the EDS. Though these sulfoaluminate phases in the 50S20G30U cannot be identified by the XRD, there is no doubt the hollow and irregular remnant Na_2SO_4 crystal demonstrated that sulfate ions were consumed during the process of the alkali activation. The absence of sulfoaluminate phases was attributed to the pore solution with a high pH value and the limited CaO and Al_2O_3 content from

the precursor, which was discussed in the XRD. In addition, no microcracks were observed in 60S30G10U and 50S20G30U, illustrating that incorporation of the unwashed APC residues could achieve a dense matrix.

Based on EDS analysis, the major elements in the AAMs were O, Si, Ca, Al and Na and this implies that the reaction products were the coexistence of the C-A-S-H and N-(C)-A-S-H gels. The sulfur and chlorine from the unwashed APC residues were detected in the gel phase of the AAMs, meaning that the C-A-S-H gels helped immobilize the sulfate and chloride ions. The Ca/Si, Si/Al and Na/Ca ratios of the gel matrix are calculated using data of 20 points, and the results are shown in Table 4 and the standard deviations of the results are less than 0.02. From Table 4, the Ca/Si, Si/Al and Na/Ca ratios of precursors and gel matrixes showed an obvious difference, meaning the occurrence of the alkali-activated reaction. An obvious reduction could be seen in the gel matrixes of Al/Si ratio, meaning that the minor content of aluminium dissolved to form the gel matrixes. The main reaction products of alkali-activated slag were C-(A)-S-H gels with a Ca/Si ratio of 0.8-1.1, this compiled well with other work (Ben et al., 2011). The incorporation of the GP and APC residues could provide Na, so the Na/Al of the AAMs matrix was increased and the Ca/Si and Al/Si ratios were reduced. The results implied that the higher amount of Na from the GP and APC residues could be incorporated into the C-A-S-H phase (with a tobermorite-like structure) and less Ca was released from the slag, which may form the N-(C)-A-S-H gels (with a three-dimensional network) in the matrix (Chitsaz et al., 2020; Puertas et al., 2011; Sun et al., 2020). In the pure C-(A)-S-H gels, the residual charge can be negative, neutral or positive, which are dependent on the Ca/Si ratio. The excessive calcium within the interlayer structures can shift the overall charge balance of C-(A)-S-H from negative to positive. Incorporation of the APC residue and GP decreased the Ca/Si ratio of AAMs, meaning the overall charge of AAMs gels may be negative, and thus the low Ca/Si ratio benefited the adsorption of heavy metals to compensate for the net negative charge. In addition, according to the electric double layer theory, the replacement of Si by Al would lead to the sorption of metal ions onto the interlayer structures of the C-(A)-S-H gels to balance the excess charges (Sun et al., 2022b; Plusquellec et al., 2016). The AAMs washed APC residues showed a higher Al/Si ratio than that of the unwashed APC residues, showing that more reactive Al from the washed APC residue could participate in the gel matrix of the AAMs. The lower Ca/Si and higher Al/Si ratio in the AAMs prepared with the washed APC residues might further enhance the adsorption of heavy metals, which resulted in lower leaching of heavy metals as shown in Table 3.

Table 4 The chemical composition of the AAMs before and after an alkali-activated reaction

No.	Matrixes (by EDS)	Precursors (by theoretical calculation)

	Na/Al	Al/Si	Ca/Si	Na/Al	Al/Si	Ca/Si
100S	0.69	0.57	1.16	0.54	2.25	0.90
50S50G	1.78	0.37	0.82	2.29	5.57	0.42
60S30G10W	2.05	0.47	0.50	1.51	3.79	0.54
60S30G10U	2.16	0.32	0.36	2.01	3.98	0.53
50S20G30W	1.11	0.39	0.70	1.46	3.15	0.56
50S20G30U	1.64	0.20	0.51	3.10	3.60	0.54

4. Conclusions

The APC residues generated from the sewage sludge incineration process were detrimental to the environment due to its rich soluble sulfate and chloride salts (e.g., NaCl and Na_2SO_4) and toxic heavy metal contents. This study explored recycling and reusing the washed and unwashed APC residues as precursors and weak alkaline activators for producing AAMs as sustainable and low carbon footprint construction materials. The effect of the washed and unwashed APC residues on the physical properties and microstructure of the AAMs was investigated. The main conclusions can be summarized below:

(a) Pre-washing by using a low L/S ratio could remove the sulfate of the as-received APC residues, while the removal of heavy metals and chlorine required a higher L/S ratio. The sulfate from the as-received APC residues could reduce the drying shrinkage of the AAMs and promote the development of long-term compressive strength.

(b) Incorporating unwashed and washed APC residues reduced the compressive strength of the AAMs mortar due to their low reactivity, but the later compressive strength could achieve a stable gain. For unwashed APC residues, the mix proportion region with a relatively higher strength of AAMs was 80-90% slag, 0-20% GP and less than 5% unwashed APC residues. For washed APC residues, the highest strength was achieved with 70-90% slag, 0-30% GP and less than 20% washed APC residues.

(c) The alkali-activated slag showed a high drying shrinkage of more than 10,000 micro strains. However, incorporating the unwashed and washed APC residues could reduce the drying shrinkage because the presence of sulfate contributed to the formation of expansive ettringite to compensate for shrinkage. The lowest drying shrinkages were about 1400 micro strains when unwashed and washed APC residues were added.

(d) In the alkali-activated slag/GP, the main reaction products were the C-A-S-H and N-(C)-A-S-H gels, and a small number of ettringite and Friedel's salts was found when the APC residues were added. The Na/Al in the gel matrix of AAMs prepared with the unwashed APC residues was increased due to the supply of sodium by the unwashed APC residues. The AAMs prepared with the washed APC residues showed a higher Al/Si ratio than that of the unwashed APC residues, showing that more reactive Al was in the AAMs matrix.

(e) The recycling of the APC residues in AAMs not only reduced the burden of landfills but also enhanced the utilization of waste as a recoverable resource. The leaching test indicated that

the AAM prepared with the washed APC residues posed little harm to the environment. But the unwashed APC residues still required to be further treated before they could be largely reused because of the high heavy metal contents.

Further studies are needed to treat the wastewater resulting from the washing of the APC residues, especially as it contains high contents of chlorine/sulfate and a low amount of heavy metals. The heavy metals concentration can be reduced to an acceptable level by pH adjustment and filtration. The predominantly sulfate/chlorine salts can be recovered from the ACP residues-washing wastewater using appropriate techniques, such as evaporation and the recovered sulfate/chlorine salts can be used by the chemical industry.

Acknowledgments

This study work was supported by a grant from the Research Grants Council (NO. P0033406) and The Hong Kong Polytechnic University.

References

Ali, H., Xuan, D., Poon, C., 2020. Assessment of long-term reactivity of initially lowly-reactive solid wastes as supplementary cementitious materials (SCMs). Constr Build Mater 232, 117192.

ASTM C1437, 1999. Standard test method for flow of hydraulic cement mortar, ASTM C1437-01, ASTM International.

ASTM C109/C109M-05, 2005. Standard test method for compressive strength of hydraulic cement mortars, ASTM C109M-05, ASTM International.

Bakharev, T., Sanjayan, J., Cheng, Y., 1999. Effect of elevated temperature curing on properties of alkali-activated slag concrete. Cem Concr Res 29(10), 1619-1625.

Bayuseno, A., Schmahl, W., 2011. Characterization of MSWI fly ash through mineralogy and water extraction. Resour Conserv Recy 55(5), 524-534.

Ben Haha, M., Le Saout, G., Winnefeld, F., Lothenbach, B., 2011. Influence of activator type on hydration kinetics, hydrate assemblage and microstructural development of alkali activated blast-furnace slags. Cem Concr Res 41(3), 301-310.

Bogush, A., Stegemann, J., Roy, A., 2019a. Changes in composition and lead speciation due to water washing of air pollution control residue from municipal waste incineration. J Hazard Mater 361, 187-199.

Bogush, A., Stegemann, J., Wood, I., Roy, A., 2015b. Element composition and mineralogical characterisation of air pollution control residue from UK energy-from-waste facilities. Waste Manage, 36: 119-129.

Brough, A., Holloway, M., Sykes J., Atkinson A,. 2000. Sodium silicate-based alkali-activated slag mortars: Part II. The retarding effect of additions of sodium chloride or malic acid. Cem Concr Res 30(9):1375-1379.

Cai, Y., Xuan, D., Poon, C., 2022. Influence of availability of calcium on the hydration of tricalcium aluminate (C_3A) in seawater mixed C_3A-gypsum system. J Am Ceram Soc 105, 5895-5910.

574 Cai, Y., Xuan, D., Hou, P., Shi, J., Poon, C., 2021. Effect of seawater as mixing water on the
575 hydration behaviour of tricalcium aluminate. Cem Concr Res 149, 106565.
576 Chen, Y., Fan, T., Wang, L., Cheng, T., Chen, S., Yuan, M., Cheng, S., 2020. Application of
577 Fenton method for the removal of organic matter in sewage sludge at room temperature. Sustain
578 12(4),1518-1528.
579 Chen, Z., Li, J., Zhan, B., Sharma, U., Poon, C., 2018. Compressive strength and
580 microstructural properties of dry-mixed geopolymer pastes synthesized from GGBS and
581 sewage sludge ash. Constr Build Mater 182, 597-607.
582 Chitsaz, S., Tarighat, A., 2020. Molecular dynamics simulation of NASH geopolymer macro
583 molecule model for prediction of its modulus of elasticity. Constr Build Mater 243, 118176.
584 Chimenos, J., Fernández, A., Cervantes, A., Miralles, L., Fernández, M., Espiell, F., 2005.
585 Optimizing the APC residue washing process to minimize the release of chloride and heavy
586 metals. Waste Manage, 25(7): 686-693.
587 Collins, F., Sanjayan, J., 2001. Microcracking and strength development of alkali activated
588 slag concrete. Cement Concrete Comp 23(4-5), 345-352.
589 Davidovits, J., 2013. Geopolymer cement. A review. Geopolymer Institute, Technical papers
590 21, 1-11.
591 Diab, A., Mohamed, I., Aliabdo, A., 2016. Impact of organic carbon on hardened properties
592 and durability of limestone cement concrete. Constr Build Mater, 102: 688-698.
593 Duxson, P., Fernández-Jiménez, A., Provis, J., Lukey, G., Palomo, A., Deventer, J., 2007.
594 Geopolymer technology: the current state of the art. J Mater Sci 42(9), 2917-2933.
595 Garcia-Lodeiro, I., Palomo, A., Fernández-Jiménez, A., Macphee, D., 2011. Compatibility
596 studies between N-A-S-H and C-A-S-H gels. Study in the ternary diagram Na_2O-CaO-Al_2O_3-
597 SiO_2-H_2O. Cem Concr Res 41(9), 923-931.
598 Gunasekara, C., Law, D., Bhuiyan, S., Setunge, S., Ward, L., 2019. Chloride induced
599 corrosion in different fly ash based geopolymer concretes. Constr Build Mater 200, 502-513.
600 Hadas, E., 2021. Economic cost-benefit analysis for the agricultural use of sewage sludge
601 treated with lime and fly ash. Int J Coal Sci Technol 8(5), 1099-1107.
602 He, P., Zhang, B., Lu, J., Poon, C., 2020a. A ternary optimization of alkali-activated cement
603 mortars incorporating glass powder, slag and calcium aluminate cement. Constr Build Mater
604 240, 117983
605 He, P., Zhang, B., Lu, J., Poon, C., 2021b. Reaction mechanisms of alkali-activated glass
606 powder-ggbs-CAC composites. Cem Concr Compos 122, 104143.
607 Hu, X., Shi, Z., Shi, C., Wu, Z., Tong, B., Ou, Z., Schutter, G., 2017. Drying shrinkage and
608 cracking resistance of concrete made with ternary cementitious components. Constr Build
609 Mater 149, 406-415.
610 Hubler, M., Thomas, J., Jennings, H., 2011. Influence of nucleation seeding on the hydration
611 kinetics and compressive strength of alkali activated slag paste. Cem Concr Res 41(8), 842-846.
612 Kourti, I., Rani, D., Deegan, D., Boccaccini, A., Cheeseman, C., 2010. Production of
613 geopolymers using glass produced from DC plasma treatment of air pollution control (APC)
614 residues. J Hazard Mater 176(1-3), 704-709.
615 Krumgalz, B., 2017. Temperature dependence of mineral solubility in water. Part I. Alkaline
616 and alkaline earth chlorides. J Phys Chem 46(4), 043101.
617 Lampris, C., Stegemann, J., Cheeseman, C., 2009. Solidification/stabilisation of air pollution
618 control residues using Portland cement: Physical properties and chloride leaching. Waste
619 Manage 29(3), 1067-1075.

Liang, G., Li, H., Zhu, H., Liu, T., Chen, Q., Guo, H., 2021. Reuse of waste glass powder in alkali-activated metakaolin/fly ash pastes: Physical properties, reaction kinetics and microstructure. Resour Conserv Recy 173, 105721.

Ling, T., Poon, C., Wong, H., 2013. Management and recycling of waste glass in concrete products: Current situations in Hong Kong. Res Conserv Recy 70, 25-31.

Liu, Y., Shi, C., Zhang, Z., Li, N., 2019. An overview on the reuse of waste glasses in alkali-activated materials. Resour Conserv Recy 144, 297-309.

Longhi, M., Rodríguez, E., Bernal, S., Provis, J., Kirchheim, A., 2022. Binary alkali-activated systems obtained by the valorisation of calcined kaolin sludge and bottom ash. Adv Cem Rese 34(2), 67-79.

Mobasher, N., Bernal, S., Provis, J., 2016. Structural evolution of an alkali sulfate activated slag cement. J Nucl Mater 468, 97-104.

Nagataki, S., Gomi, H., 1998. Expansive admixtures (mainly ettringite). Cem Concr Comp 20(2-3), 163-170.

Nguyen, H., Adesanya, E., Ohenoja, K., Kriskova, L., Pontikes, Y., Kinnunen, P., Illikainen, M., 2019. Byproduct-based ettringite binder-A synergy between ladle slag and gypsum. Constr Build Mater 197, 143-151.

Pan, S., Tseng, D., Lee, C., 2003. Influence of the fineness of sewage sludge ash on the mortar properties. Cem Concr Res 33(11), 1749-1754.

Pascual, A., Tognonvi, T., Tagnit-Hamou, A., 2021. Optimization study of waste glass powder-based alkali activated materials incorporating metakaolin: Activation and curing conditions. J Clean Prod 308, 127435.

Patel, Y., Shah, N., 2018. Development of self-compacting geopolymer concrete as a sustainable construction material. Sustain Environ Res 28(6), 412-421.

Plusquellec, G., Nonat, A., 2016. Interactions between calcium silicate hydrate (C-S-H) and calcium chloride, bromide and nitrate. Cem Concr Res 90, 89-96.

Provis, J., Deventer, J., 2009. Geopolymers: structures, processing, properties and industrial applications. Elsevier Published.

Puertas, F., Palacios, M., Manzano, H., Dolado, J., Rico, A., Rodríguez, J., 2011. A model for the CASH gel formed in alkali-activated slag cements. J Eur Ceram Soc 31(12), 2043-2056.

Quina, M., Bordado, J., Quinta-Ferreira, R., 2010a. Chemical stabilization of air pollution control residues from municipal solid waste incineration. J Hazard Mater 179(1-3), 382-392.

Quina, M., Bordado, J., Quinta-Ferreira, R., 2008b. Treatment and use of air pollution control residues from MSW incineration: An overview. Waste Manage 28(11), 2097-2121.

Rani, D., Boccaccini, A., Deegan, D., Cheeseman, C., 2008a. Air pollution control residues from waste incineration: Current UK situation and assessment of alternative technologies. Waste Manage 28(11), 2279-2292.

Rani, D., Gomez, E., Boccaccini, A., Hao, L., Deegan, D., Cheeseman, C., 2008b. Plasma treatment of air pollution control residues. Waste Manage 28(7), 1254-1262.

Redden, R., Neithalath, N., 2014. Microstructure, strength, and moisture stability of alkali activated glass powder-based binders. Cement Concrete Comp 45, 46-56.

Ren, P., Ling, T., 2021. Roles of chlorine and sulfate in MSWIFA in GGBFS binder: Hydration, mechanical properties and stabilization considerations. Environ Pollut 284, 117175.

Shi, C., Qian, J., 2000. High performance cementing materials from industrial slags-a review. Res Conserv Recy 29(3), 195-207.

Shoaei, P., Ameri, F., Musaeei, H., Ghasemi, T., Ban, C., 2020. Glass powder as a partial precursor in Portland cement and alkali-activated slag mortar: A comprehensive comparative study. Constr Build Mater 251(10), 118991.

Sun, K., Ali, H.A., Xuan, D., Ban, J., Poon, C., 2022a. Utilization of APC residues from sewage sludge incineration process as activator of alkali-activated slag/glass powder material. Cement Concrete Comp 133, 104680.

Sun, K., Peng, X., Chu, S., Wang, S., Zeng, L., Ji, G., 2021. Utilization of BOF steel slag aggregate in metakaolin-based geopolymer. Constr Build Mater 300(20), 124024.

Sun, K., Peng, X., Wang, S., Zeng, L., 2019. Design method for the mix proportion of geopolymer concrete based on the paste thickness of coated aggregate. J Clean Prod 232, 508-517.

Sun, K., Peng, X., Wang, S., Zeng, L., Ran, P., Ji, G., 2020. Effect of nano-SiO_2 on the efflorescence of an alkali-activated metakaolin mortar. Constr Build Mater 253(30), 118952.

Sun, K., Xuan, D., Li, J., Ji, G., Poon, C., Wang, S., Peng, X., Lv, X., Zeng, G., 2022b. Effect of the Ti-extracted residue on compressive strength and microstructural properties of modified cement mortar. Constr Build Mater 320(21), 126190.

Swann, L., Downs, D., Waye, M., 2017. Waste to energy solution-the sludge treatment facility in Tuen Mun, Hong Kong. Energy Procedia 143, 500-505.

Thaulow, N., Sahu, S., 2004. Mechanism of concrete deterioration due to salt crystallization. Mater Charact 53(2-4), 123-127.

Uppalapati, S., Vandewalle, L., Cizer, O., 2020. Autogenous shrinkage of slag-fly ash blends activated with hybrid sodium silicate and sodium sulfate at different curing temperatures. Constr Build Mater 265, 121276.

Van Sande, J., Peys, A., Hertel, T., Rahier, H., Pontikes, Y., 2020. Upcycling of non-ferrous metallurgy slags: Identifying the most reactive slag for inorganic polymer construction materials. Res Conserv Recy 154, 104627.

Walkley, B., San Nicolas, R., Sani, M., Rees, G., Hanna, J., van Deventer, J., Provis, J., 2016. Phase evolution of C-(N)-ASH/NASH gel blends investigated via alkali-activation of synthetic calcium aluminosilicate precursors. Cem Concr Res 89, 120-135.

Wang, L., Jin, Y., Nie, Y., Li, R., 2010. Recycling of municipal solid waste incineration fly ash for ordinary Portland cement production: A real-scale test. Res Conserv and Recy 54(12), 1428-1435.

Yang, Z., Tian, S., Ji, R., Liu, L., Wang, X., Zhang, Z., 2017. Effect of water-washing on the co-removal of chlorine and heavy metals in air pollution control residue from MSW incineration. Waste Manage 68, 221-231.

Zhang, B., He, P., Poon, C., 2020. Optimizing the use of recycled glass materials in alkali activated cement (AAC) based mortars. J Clean Prod 255, 120228.